Electronic Supplementary Information

High-performance electrocatalytic nitrate reduction into ammonia by chitosan regulated Co nanocatalyst

Yaqian Xin,[ab] Shengbo Zhang,*[ab] Jiafang Liu,[ab] Yong Jiang,[c] Yunxia Zhang,[ab] Guozhong Wang,[ab] and Haimin Zhang*[ab]

[a] Key Laboratory of Materials Physics, Centre for Environmental and Energy Nanomaterials, Anhui Key Laboratory of Nanomaterials and Nanotechnology, CAS Center for Excellence in Nanoscience Institute of Solid State Physics, HFIPS, Chinese Academy of Sciences Hefei 230031, PR China

[b] University of Science and Technology of China

[c] Shanghai Synchrotron Radiation Facility, Shanghai Advanced Research Institute, Chinese Academy of Sciences, Shanghai 201800, PR China

* Corresponding author: E-mail: zhanghm@issp.ac.cn, shbzhang@issp.ac.cn

Experimental Section

Chemicals

Chitosan, Cobalt chloride hexahydrate ($CoCl_2 \cdot 6H_2O$, AR, 99%), K_2SO_4 (AR, 99.0%), NaOH (96.0%), sodium nitroferricyanide(III) dehydrate ($C_5FeN_6Na_2O \cdot 2H_2O$, AR, 99.0%), salicylic acid ($C_7H_6O_3$, AR, 99.5%), N-(1-naphthyl) ethylenediamine dihydrochloride ($C_{10}H_7NHC_2H_4NH_2 \cdot 2HCl$, AR, 95.0%), thiosemicarbazide (CH_5N_3S, AR, 99.0%), sulfanilamide ($NH_2C_6H_4SO_2NH_2$, AR, 95.0%), $^{15}KNO_3$ (AR), $(^{15}NH_4)_2SO_4$ (AR), D_2O(99.9 atom% D) were all purchased from Shanghai Aladdin Biochemical Technology Co., Ltd. NaClO (AR, 6-14% active chlorine base), NH_4Cl (AR, 99.5%) were purchased from Shanghai Aladdin Bio-Chem Technology Co., Ltd. Sodium citrate ($C_6H_5Na_3O_7 \cdot 2H_2O$, AR, 99.0%), KNO_3 (AR) were purchased from Sinopharm Chemical Reagent Co.,Ltd. The water used for all solutions was purified through a Millipore system (Millipore Corp., 18.2 MΩ cm). Commercial carbon paper (CP, HCP030N) was purchased from Shanghai Hesen Electric Co. Ltd. All chemicals were used as received without further purification.

Synthesis of CC

6.0 g chitosan powder was ground and pyrolyzed at 900 ℃for 1 hour under Ar atmosphere with a heating rate of 3 ℃ min^{-1} in a tubular furnace. After cooling to room temperature, wash the dark solid powder with deionized water and ethyl alcohol several times. Finally, the catalyst was collected by centrifugation and dried overnight.

Synthesis of Co-NPs/CC

6.0 g chitosan powder and 0.25 M $CoCl_2 \cdot 6H_2O$ were added into 100 mL deionized water with stirring at 80 ℃ for 12 h to dry the solution into the solid mixture. Then, pyrolyzed in a tubular furnace under Ar atmosphere with a heating rate of 3 ℃ min^{-1} to 900 ℃ and kept for1 hour. After cooling down to room temperature, the resulting dark solid powder was collected by centrifugation and then dried in the oven overnight after washing by deionized water and ethyl alcohol for several times.

Material Characterization

The scanning electron microscopy (SEM) images were obtained using SU8020 (Hitachi, Japan). The transmission electron microscopy (TEM) images were obtained using JEMARM 200F. The aberration-corrected high-angle annular dark-field scanning transmission electron microscopy (HAADF-STEM) measurements andenergy-dispersive X-ray (EDX) spectroscopy were performed using JEM-ARM200F. X-ray diffraction (XRD) patterns were acquired using Philips X'pert PRO with Cu Ka radiation (λ = 1.5418 Å) at 40 kV and 40 mA. Nitrogen adsorption-desorption isotherms were measured using Autosorb-iQ-Cx. X-ray photoelectron spectroscopy (XPS) analysis was performed on an ESCALAB 250 X-ray photoelectron spectrometer (Thermo, America). The content of metallic Co was quantitatively determined by ICP-AES (ICP-6300, Thermo Fisher Scientific). *In situ* attenuated total reflection surface-enhanced infrared adsorption spectroscopy (ATR-SEIRAS) measurements were conducted by a Nicolet Nexus FT-IR spectrometer. The synchrotron-based X-ray absorption near-edge structure (XANES) and the extended X-ray absorption fine structure (EXAFS) measurements were performed at the BL05U station of Shanghai Synchrotron Radiation Facility, China.

Electrochemical measurements

All the electrochemical measurements were performed on a CHI 660E electrochemical workstation (CH Instrumental Corporation, Shanghai, China) using an H-type cell, which was separated by a Nafion 211 proton exchange membrane. The Nafion 211 membrane was treated at 80 ℃ in H_2O_2(5 wt.%) and 0.5 M H_2SO_4aqueous solution in turn to protonate and then rinsed with deionized water before use. The catalyst inks were prepared by dispersing 5 mg sample into 500 μL of ethanol, 450 μL of water and 50 μL of Nafion (5 wt.%) under ultrasonic for 30 min, and then were loaded on a carbon paper (1.0×1.0 cm^2) as the working electrode with 1mg cm^{-2} catalyst. The saturated Ag/AgCl electrode was used as the reference electrode and a platinum mesh was used as the counter electrode. Before use, the

working electrode was activated in 0.1 M K_2SO_4 +0.1 M KNO_3 solution. Unless otherwise stated, all experiments were performed in 0.1 M K_2SO_4 +0.1 M KNO_3 solution. All measured potentials versus Ag/AgCl were transformed into the potentials versus reversible hydrogen electrode (RHE) according to the following equation:

$$E_{RHE}=E_{Ag/AgCl}+0.059pH+E^{\circ}_{Ag/AgCl}$$

where the $E_{Ag/AgCl}$ is the equilibrium potential under standard conditions and $E^{\circ}_{Ag/AgCl}$=0.197V versus RHE at 25°C.

Determination of ammonia.

The concentration of the produced ammonia was detected by the indophenol blue method.[1]In detail, taken 100 μL of electrolyte in a cathode cell after 2 h electrocatalysis, and then added 9900 μL of deionized water in a 15 ml colorimetric tube. Subsequently, 500 μL of coloring agent (composed of 10 g salicylic acid, 10g sodium citrate, 55 ml 2 M sodium hydroxide with deionized water in 200 ml solution), 100 μL of oxidizing solution (containing 5ml sodium hypochlorite and 45ml 2 M sodium hydroxide in 50 ml solution), and 100 μL of catalyst solution (1.0 g $Na_2[Fe(CN)_5NO]\cdot 2H_2O$ diluted to 100 mL with deionized water) were added to the measured sample solution in turn. After the color development for 1h at room temperature, the absorbance measurements were performed by UV-Vis spectrophotometer at a wavelength of 697.5 nm. The obtained calibration curve was used to calculate the ammonia concentration.

Determination of nitrite.

The produced nitrite in the electrolyte was detected by the Griess method.[2] In detail, the N-(1-naphthyl) ethylenediamine dihydrochloride (1 g), sulfonamide (20 g) and H_3PO_4 (50 mL, 85%) were dissolved in 250 ml of deionized water and then set the mixture to 500 ml volumetric flask to form the Griess reagent. Added 1 ml of reacted electrolyte with 9 ml of deionized water into a 15 ml colorimetric tube then mixed with 200 μL of Griess reagent and placed for 20 min at room temperature. UV-vis

spectrophotometer was used to measure the absorbance of the generated nitrite at the wavelength of 540 nm. Then the concentration of NO_2^- was obtained by the calibration curve.

Calculation of NtrRR Performance

R_{NH3}, FE and S_{NH3} are calculated by the following formulas:

$$R_{NH_3}(\mu g\ h^{-1}\ cm^{-2}) = \frac{C_{NH_3}(\mu g\ mL^{-1}) \times V(mL)}{t\ (h) * S\ (cm^2)}$$

$$FE\ (\%) = \frac{8 \times n_{NH_3}(mol) \times F\ (C\ mol^{-1})}{Q\ (C)} \times 100\%$$

$$S_{NH_3}\ (\%) = \frac{C_{NH_3\text{-}N}}{C_{NO_2^-\text{-}N} + C_{NH_3\text{-}N}} \times 100\%$$

C_{NH3} is the concentration of produced NH_3 and V is the volume of electrolyte. t is the electrolysis time, S is the area of the loaded electrocatalyst, F is the faradaic constant (96485 C mol^{-1}) and Q is the total charge transferred during electrolysis. $C_{NH3\text{-}N}$ is the concentration of produced NH_3-N and $C_{NO2^-\text{-}N}$ is the concentration of produced NO_2^--N.

R_{NO2^-} and FE are calculated by the following equations:

$$R_{NO_2^-}\ (\mu g\ h^{-1}\ cm^{-2}) = \frac{C_{NO_2^-}\ (\mu g\ mL^{-1}) \times V(mL)}{t\ (h) * S\ (cm^2)}$$

$$FE\ (\%) = \frac{2 \times n_{NO_2^-}\ (mol) \times F\ (C\ mol^{-1})}{Q\ (C)} \times 100\%$$

$C_{NO2^-}$is the measured NO_2^- concentration and V is the volume of electrolyte solution. t is the electrolysis time, S is the area of the loaded electrocatalyst, F is the faradaic constant (96485 C mol^{-1}) and Q is the total charge transferred during electrolysis.

^{15}N Isotope Labeling Experiments

^{15}N isotopic labeling experiments were conducted using 0.1 M K_2SO_4 + 0.1 M $K^{15}NO_3$ as the electrolyte with the same experimental procedure of 0.1 M K_2SO_4 + 0.1 M KNO_3 experiments. The yielded $^{15}NH_3$ was measured by the ^1H NMR methods with D_2O used as an internal standardusing Bruker Avance-400 MHz.

In situ ATR-SEIRAS Spectroscopy Measurement

The *in situ* ATR-SEIRAS was performed on a Nicolet iS50 FTIR spectrometer (Thermo Scientific) equipped with an MCT-A detector with silicon as the prismatic window and cooled by liquid nitrogen during the electrochemical process. The NtrRR was performed in a three-electrode reactor with the Ag/AgCl and Pt wire used as the reference and counter electrode. The working electrode was prepared by the following method: first, the gold film was deposited on the silicon prismatic surface by chemical deposition, then the catalyst ink was dropped on the surface of the gold film. The spectrum was recorded in the 0.1 M K_2SO_4 + 0.1 M KNO_3 electrolyte by the potential from -0.7 to -1.2 V *vs* RHE with an interval of 0.1 V. The background spectrum of the catalyst electrode was obtained at an open-circuit voltage before systematic measurement.

The online DEMS tests

The online DEMS tests were performed in 0.1 M K_2SO_4 + 0.1 M KNO_3 electrolyte solution in a three-electrode reactor with the Ag/AgCl, Pt wire, and the catalyst which dropped on abreathable film with gold plating layer used as the reference, counter，and working electrode, respectively. The potential of -1.0V *vs.* RHE was applied for 1 min after the baseline of the mass spectrometry remained stable. The differential mass signals were recorded when the gaseous products formed on the electrode surface. The next cycle began when the signal returned to baseline, using the same conditions to avoid accidental error. The one cycle lasted 6 min.

Supplementary Figures and Tables

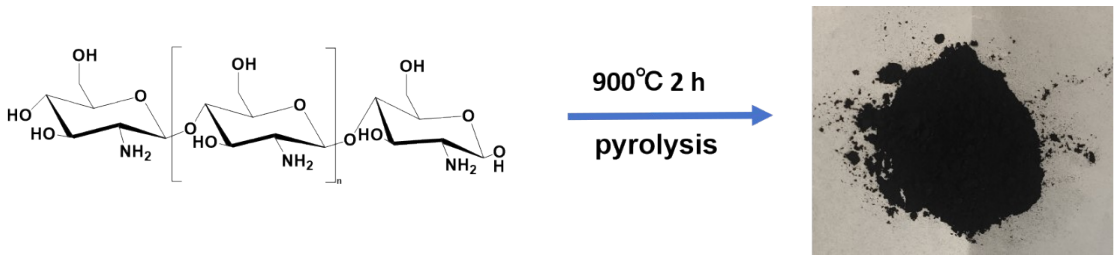

Fig. S1 Schematic illustration of the synthetic process of CC sample.

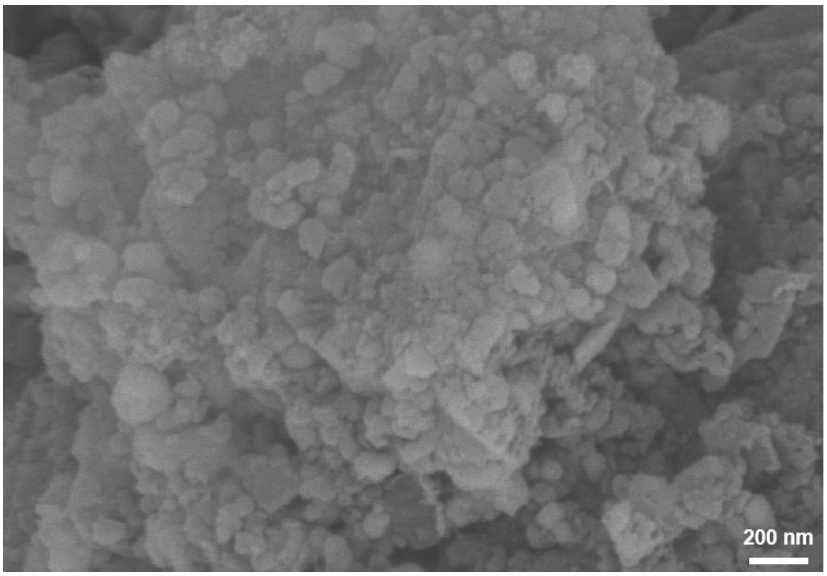

Fig. S2 SEM image of Co-NPs/CC.

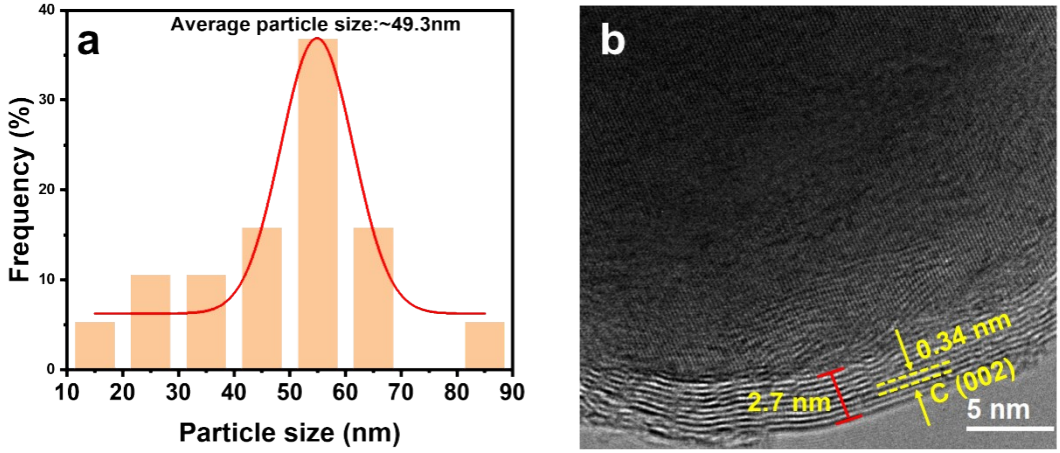

Fig. S3 (a) The particle sizes of the Co-NPs and (b) the thickness of the carbon layer for the Co-NPs-CC.

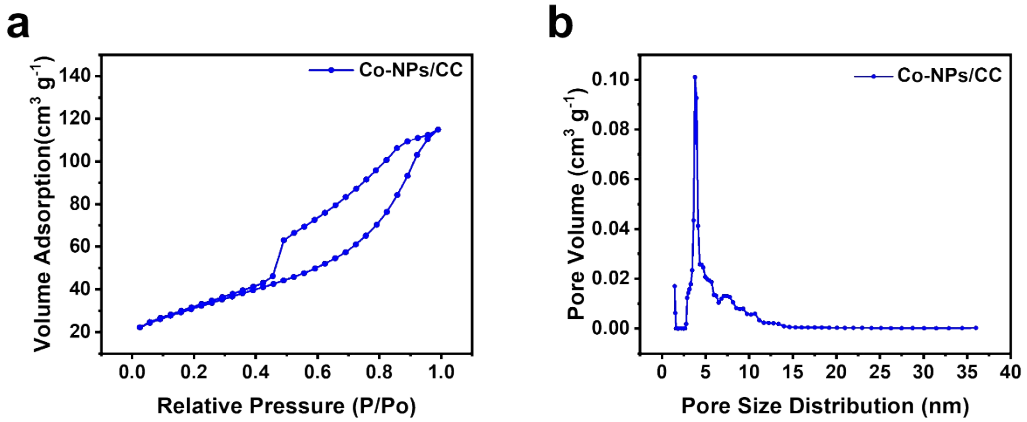

Fig. S4 (a) Nitrogen adsorption–desorption isotherm curve and **(b)** Pore size distribution curve of Co-NPs/CC.

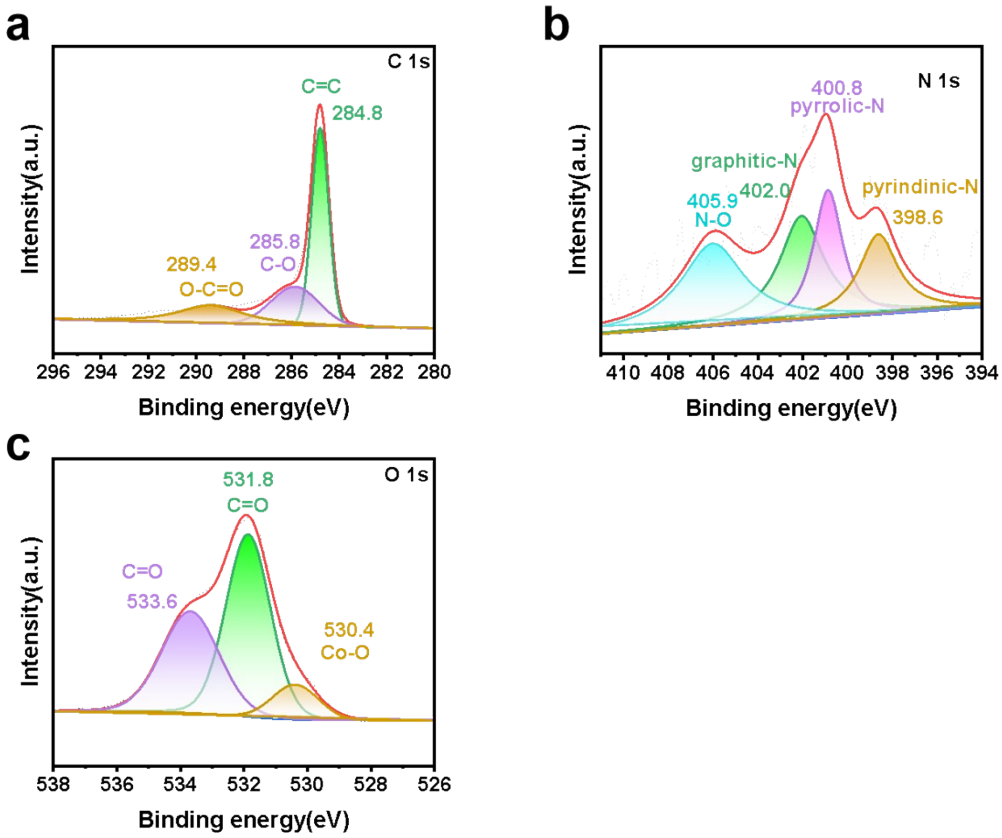

Fig. S5 High-resolution XPS spectra of **(a)** C 1S, **(b)** N 1s, **(c)** O 1s of Co-NPs/CC

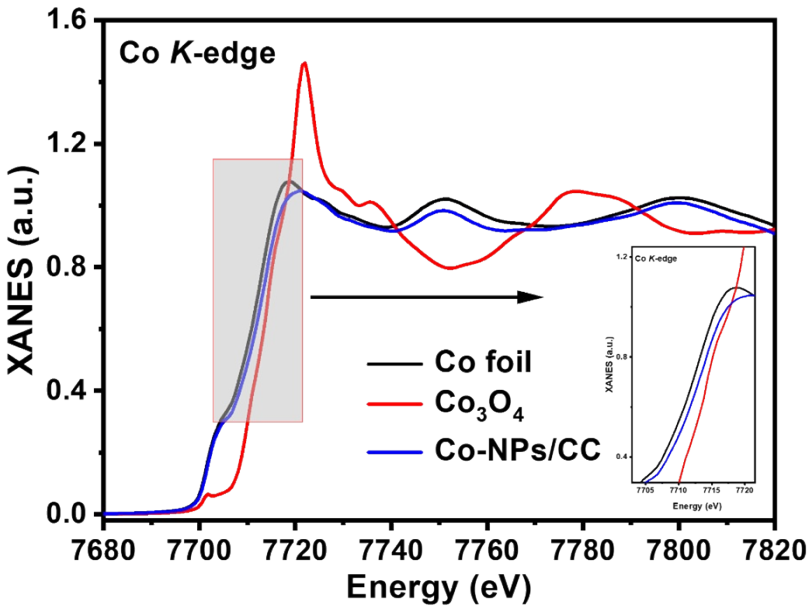

Fig. S6 Co *K*-edge XANES spectra and the corresponding partial enlarged view.

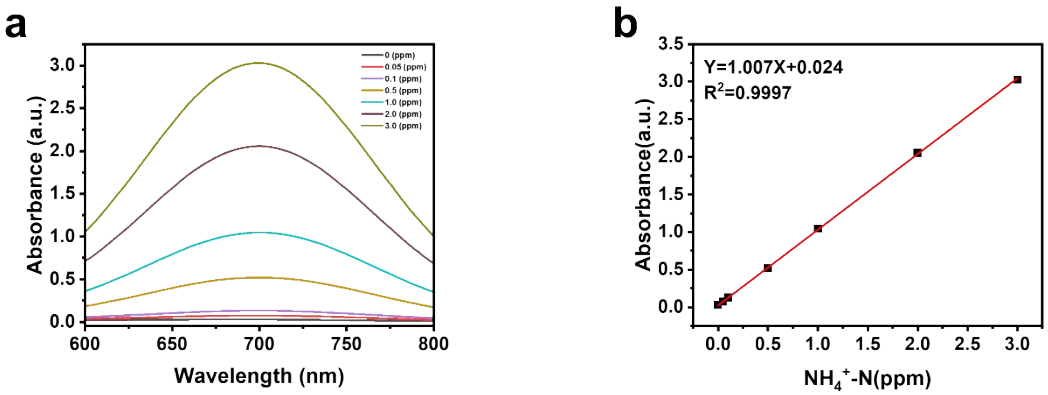

Fig. S7 (a) UV-Vis absorption spectra of various NH_4^+-N concentrations (0, 0.05, 0.1, 0.25, 0.5, 1.0, 2.0, 2.5 and 3 ppm). **(b)** The calibration curve used for calculation of NH_4^+-N concentrations.

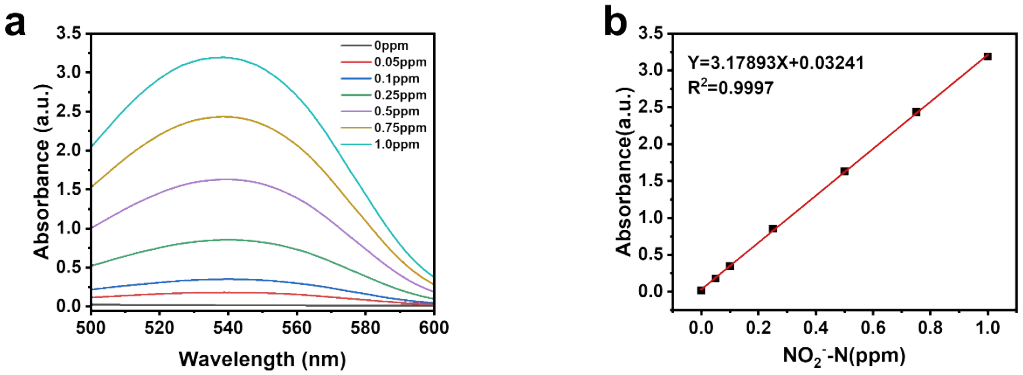

Fig. S8 (a) UV-Vis absorption spectra of various NO_2^--N concentrations (0, 0.05, 0.1, 0.25, 0.5, 0.75 and 1.0 ppm). **(b)** The calibration curve used for calculation of NO_2^--N concentrations.

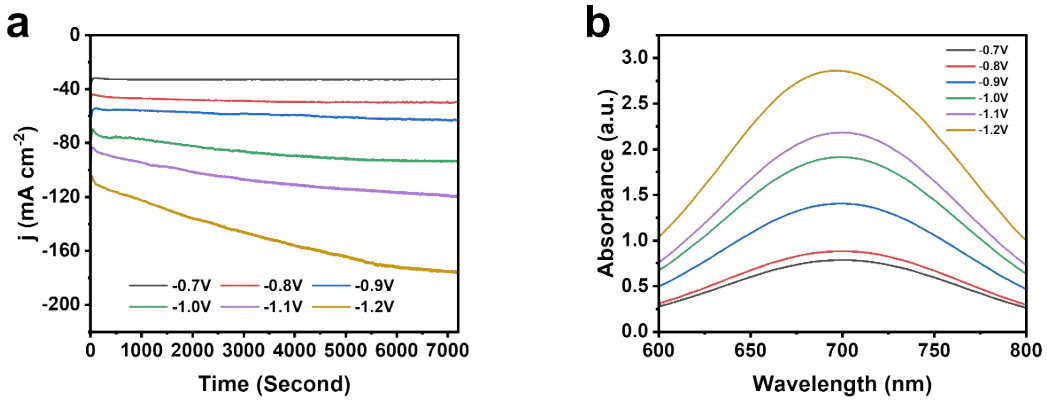

Fig. S9 (a) The j-t curves at different potentials in 0.1 M K_2SO_4 + 0.1M KNO_3 electrolyte over a 2 h period. **(b)** UV-Vis absorption spectra of the corresponding samples.

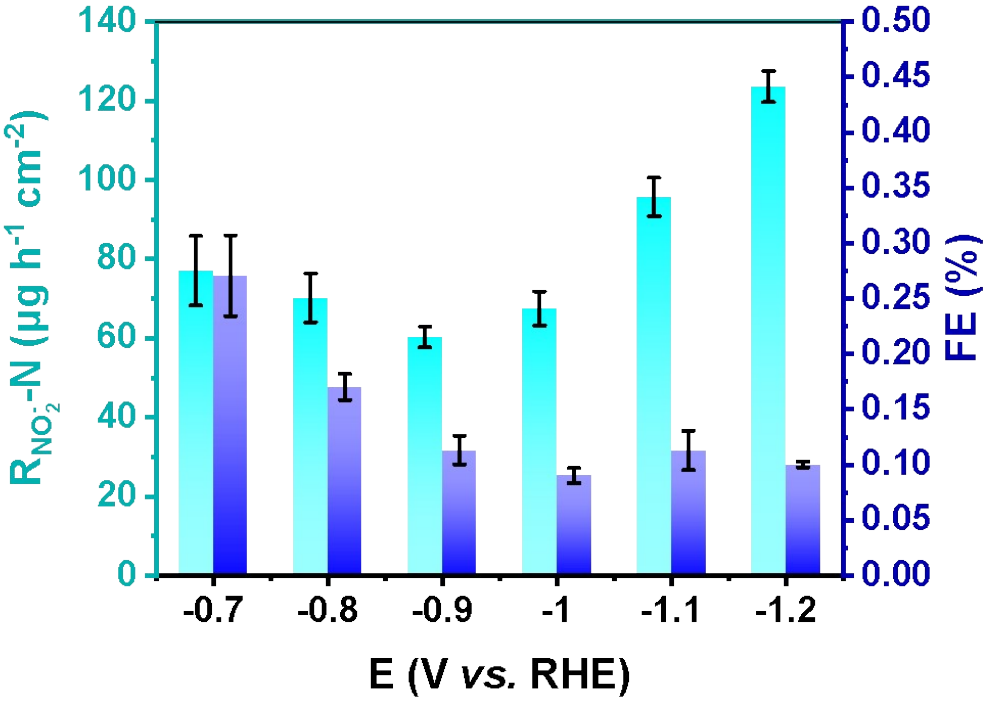

Fig. S10 The yield NO_2^--N and FE of NO_2^- in different potentials between −0.7 to −1.2 V (*vs.* RHE).

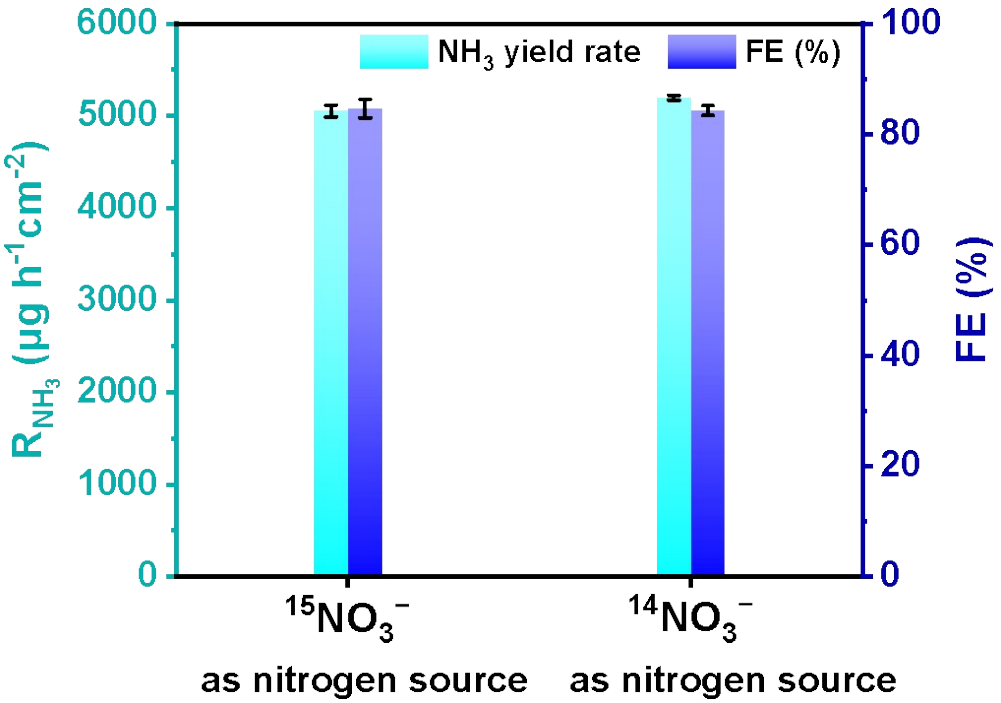

Fig. S11 Comparison chart of R_{NH3} and FE using $^{15}NO_3^-$ and $^{14}NO_3^-$ as nitrogen source.

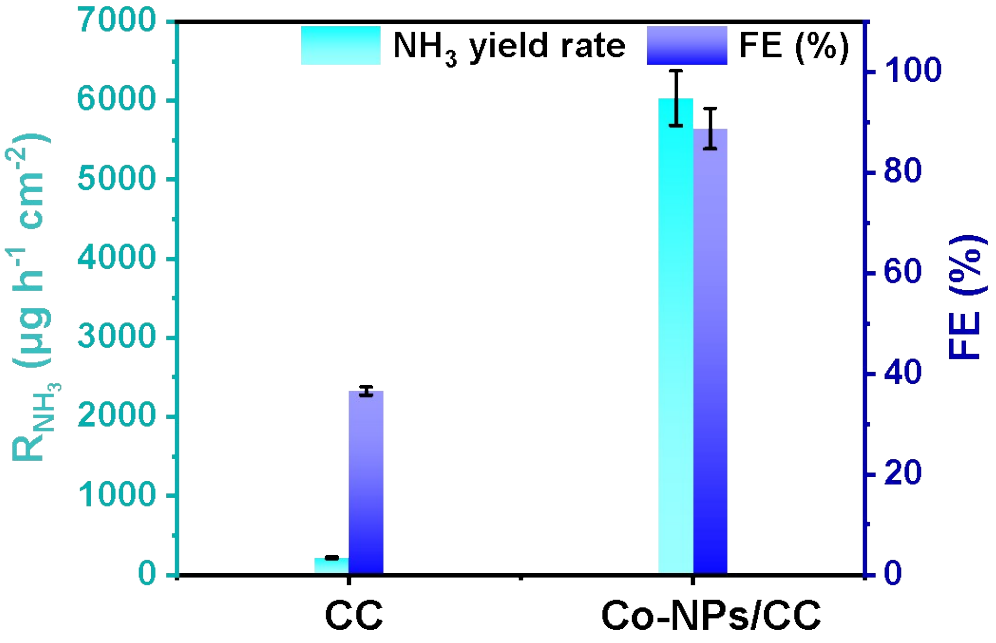

Fig. S12 R_{NH3} and FE of the electrocatalysts CC and Co-NPs/CC at -1.0 V (*vs.* RHE) for 2 h.

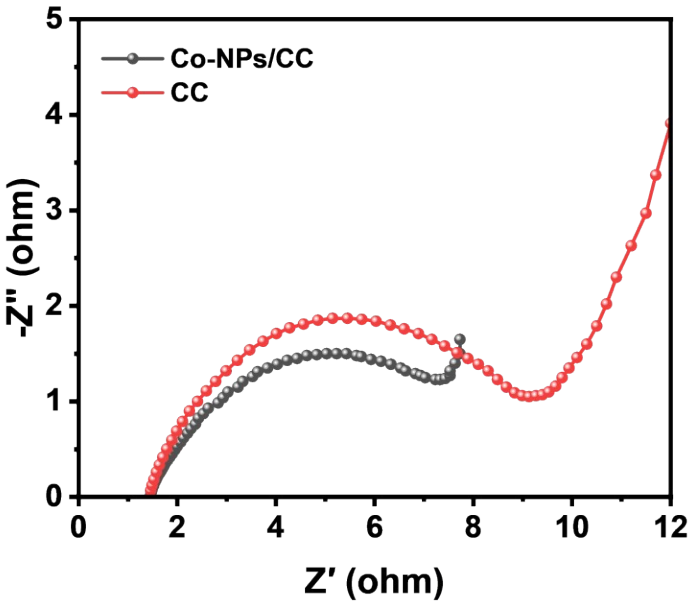

Fig. S13 The electrochemical impedance spectra of Co-NPs/CC and CC.

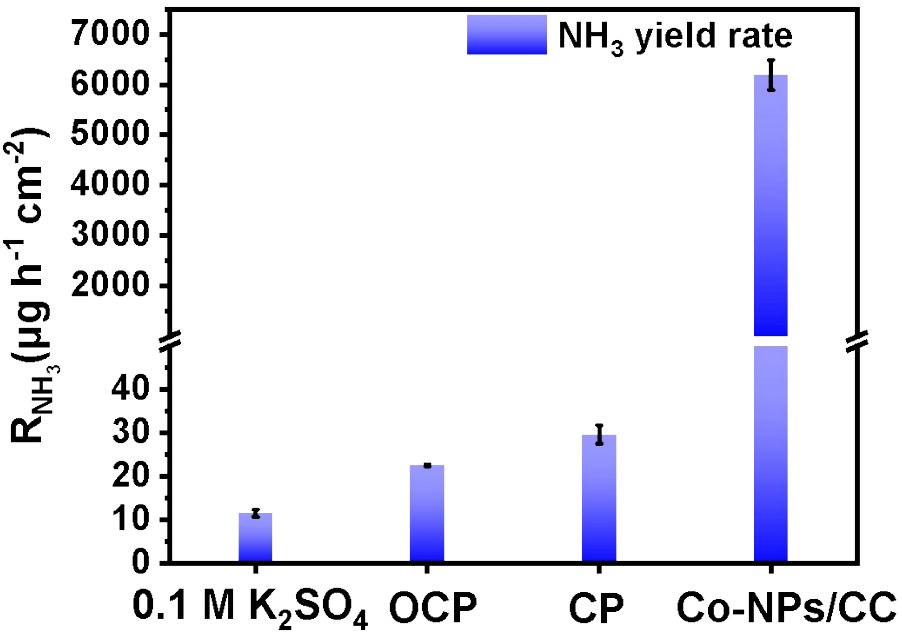

Fig. S14 R_{NH3} of contrast experiments with different conditions 0.1 M K_2SO_4, OCP, CP and Co-NPs/CC at −1.0 V (*vs.* RHE) for 2 h.

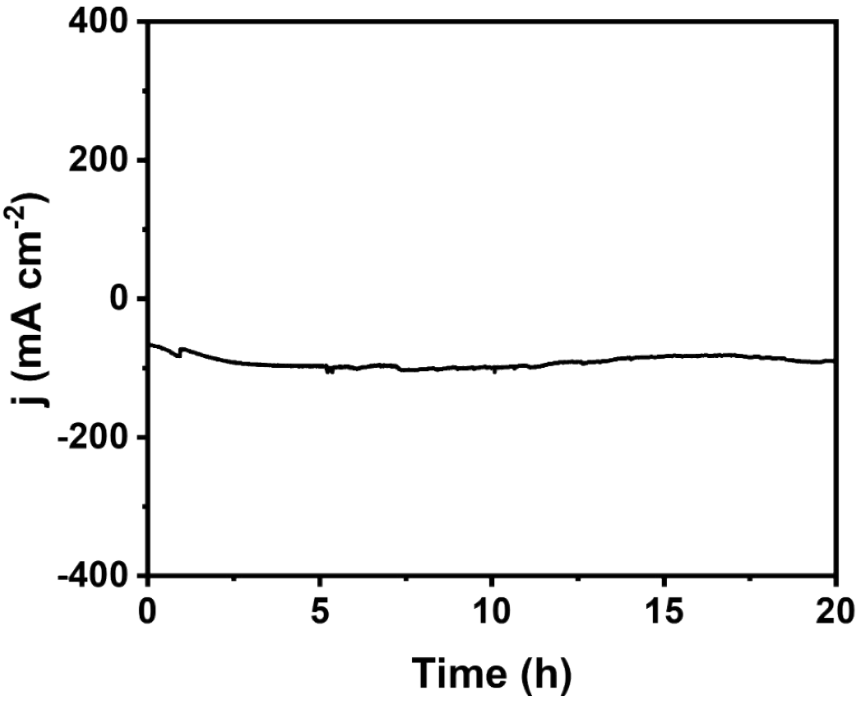

Fig. R15 The j-t curve of long-time stability test for 20h at -1.0 V *vs.* RHE.

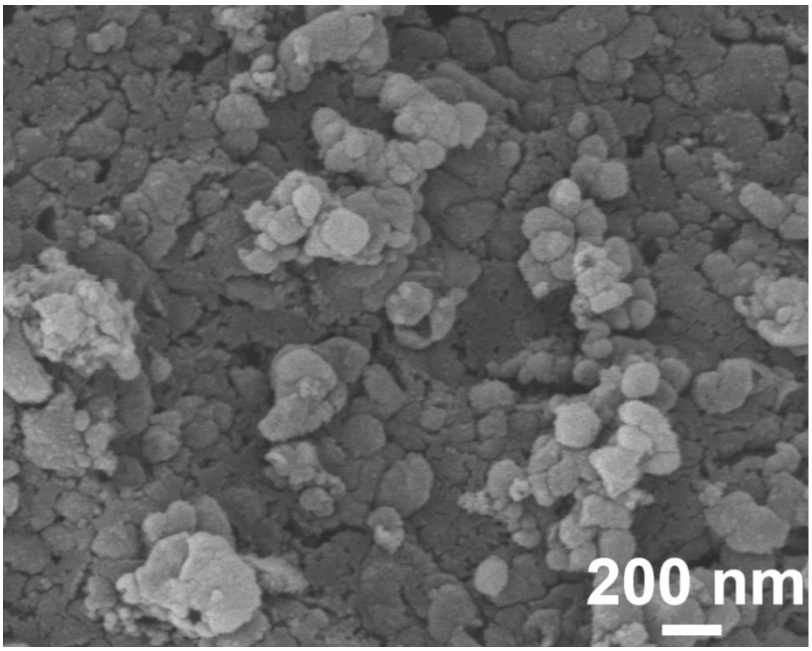

Fig. S16 SEM image of Co-NPs/CC after 8 NtrRR recycles.

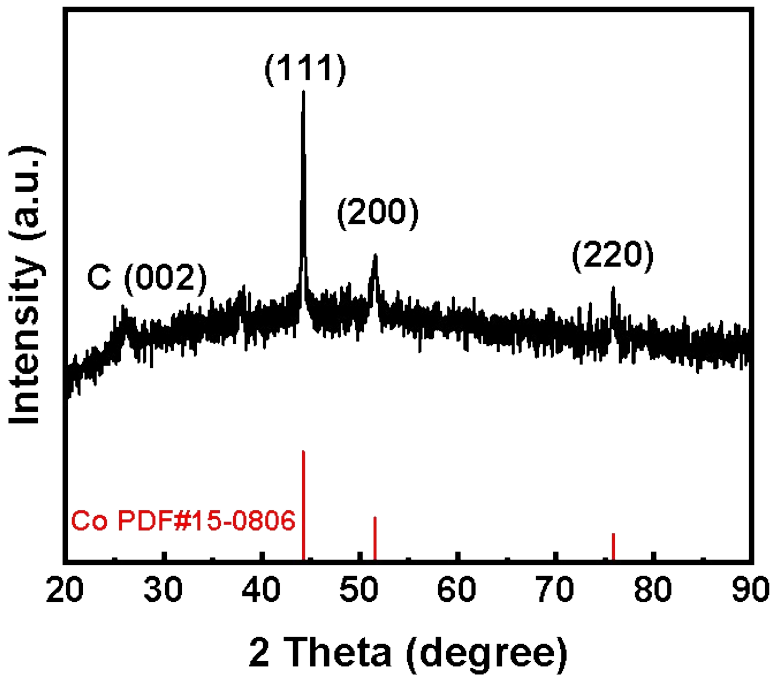

Fig. S17 XRD patterns of Co-NPs/CC after 8 NtrRR recycles

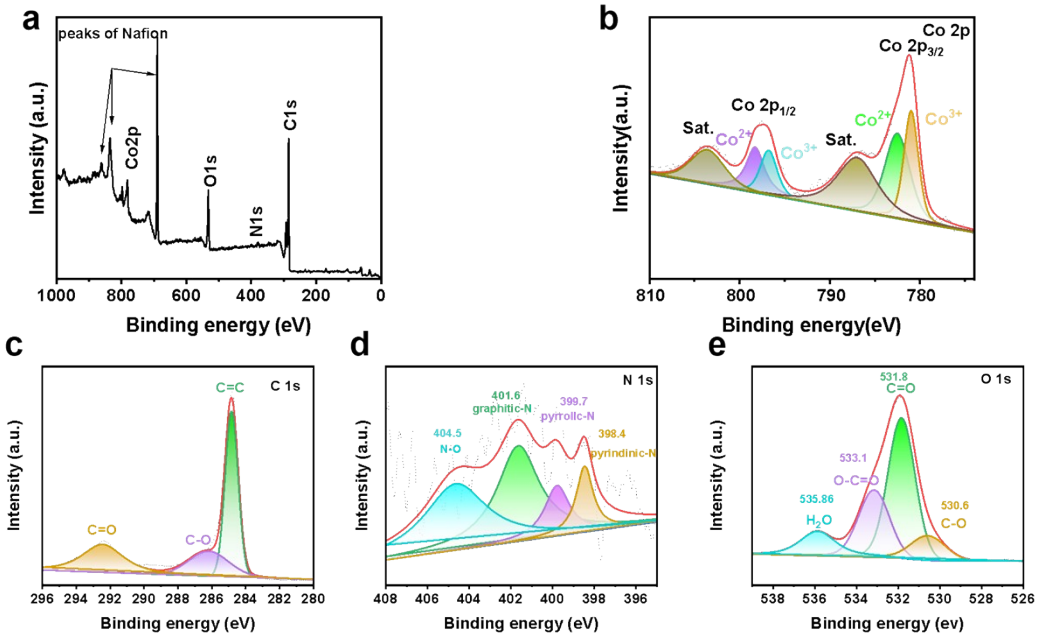

Fig. S18 (a) Survey XPS spectrum and high-resolution XPS spectra of **(b)** Co 2p, **(c)** C 1s, **(d)** N 1s and **(e)** O 1s of Co-NPs/CC after 8 NtrRR recycles.

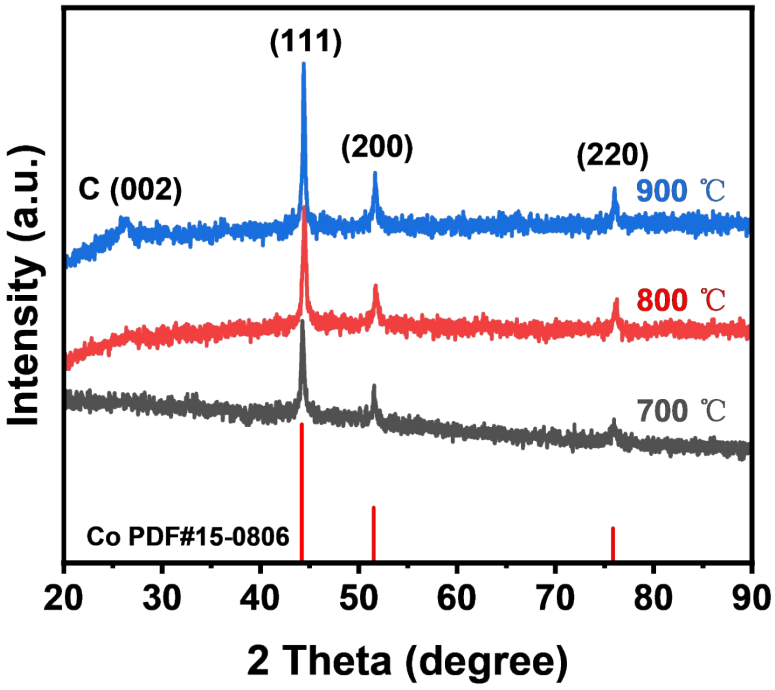

Fig. S19 XRD pattern of the Co-NPs/CC-700, Co-NPs/CC-800 and Co-NPs/CC-900.

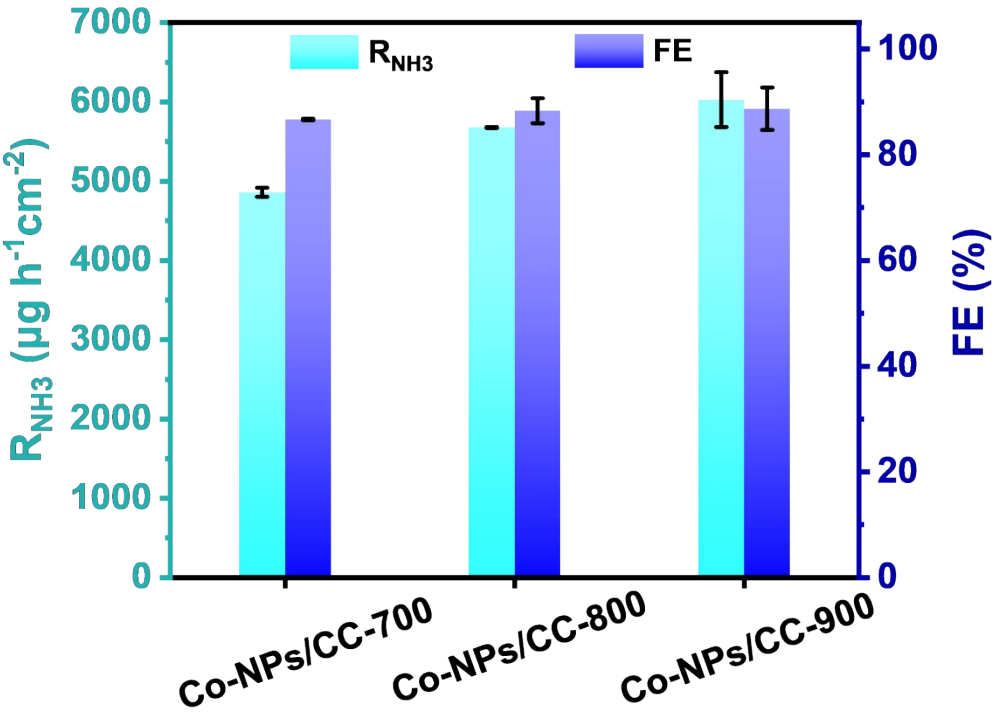

Fig. S20 R_{NH3} and FE of the electrocatalysts Co-NPs/CC-700, Co-NPs/CC-800 and Co-NPs/CC-900 at -1.0 V (*vs.* RHE) for 2 h.

Table S1. Comparison of NtrRR performance between Co-NPs/CC catalyst and others electrocatalysts recently-reported.

Catalyst	Electrolyte	NH_3 yield rate μ g h^{-1} cm^{-2}	FE (%)	Refs.
Ti	0.3 M KNO_3 0.1 M HNO_3	1850	82 (-1.0V *vs*. RHE)	3
$Cu_{0.65}Pd_{0.35}O_x$	0.1 M KNO_3	1410	74 (-0.2V *vs*. RHE)	4
Bi_2S_3/MoS_2/CC	0.1 M Na_2SO_4 0.1 M $NaNO_3$	2550	88.4 (-0.8V *vs*. RHE)	5
Cu-N-C	0.1 M KOH 0.1 M KNO_3	4500	84.7 (-1.0V *vs*. RHE)	6
a_1-Ru-CNTs	5 mM Cs_2CO_3 500 ppm $NaNO_3$	362.75	80.6 (-0.2V *vs*. RHE)	7
Co_3O_4/Co	0.1 M K_2SO_4 1000 ppm KNO_3	4430	88.7 (-0.8 V *vs*. RHE)	8
$Fe_3O_4@TiO_2$/TP	0.1 M PBS 0.1 M $NaNO_3$	12393	88.4 (-0.9 V *vs*. RHE)	9
Pd/NF	0.5 M Na_2SO_4 0.1 M $NaNO_3$	25840	78 (-1.4 V *vs*. RHE)	10
Co-Fe@Fe_2O_3	0.1 M Na_2SO_4 500 ppm $NaNO_3$	880.5	85.2 (-0.75V *vs*. RHE)	11
CuNi-NC	0.1M PBS 50 ppm $NaNO_3$	\	79.6 (-1.0V *vs*. RHE)	12
Pd-NDs/Zr-MOF	0.1M Na_2SO_4 500 ppm NO_3	1870	58.1 (-1.3V *vs*. RHE)	13
Fe single atom	0.25 M K_2SO_4 0.5 M KNO_3	7820	75 (-0.66 V *vs*. RHE)	14
Fe_2TiO_5	PBS	1241	87.6	15

	0.1M $NaNO_3$		(-0.9V *vs*. RHE)	
$CuCo_2O_4$/CFs	1.0 M KOH 0.1 M KNO_3	2703	81.9 (-0.3 V *vs*. RHE)	16
$Cu_{0.68}Ir_{0.14}O_z$	1.0 M KOH 0.1 M KNO_3	7140	87.0 (0V *vs*. RHE)	17
Cu_2O-Cu	1 M KOH 250 ppm $NaNO_3$	2170	84.38 (-0.25 V *vs*. RHE)	18
$SmCO_3$	0.1 M PBS 0.1 M $NaNO_3$	1440	81.3 (-1.0V *vs*. RHE)	19
Cu_{SA} NPC	0.01 M PBS 0.1 ppm $NaNO_3$	2602	87.2 (-1.1 V *vs*. RHE)	20
Ni_2P@Cu_3P	0.5 M K_2SO_4 200ppm KNO_3-N	4732.8	96.97 (-00.49 V *vs*. RHE)	21
This work	0.1 M K_2SO_4 0.1 M KNO_3	9181.72 ± 60.88	88.71 ± 4.02% （-1.0V *vs*. RHE)	

Reference

1. D. Zhu, L. Zhang, R. E. Ruther and R. J. Hamers, Photo-illuminated diamond as a solid-state source of solvated electrons in water for nitrogen reduction, *Nat. Mater.*, 2013, **12**, 836-841.
2. P. Li, Z. Jin, Z. Fang and G. Yu, A single-site iron catalyst with preoccupied active centers that achieves selective ammonia electrosynthesis from nitrate, *Energy Environ. Sci.*, 2021, **14**, 3522-3531.
3. J. M. McEnaney, S. J. Blair, A. C. Nielander, J. A. Schwalbe, D. M. Koshy, M. Cargnello and T. F. Jaramillo, Electrolyte engineering for efficient electrochemical nitrate reduction to ammonia on a titanium electrode, *ACS Sustainable Chem. Eng.*, 2020, **8**, 2672-2681.
4. W. Jung, J. Jeong, Y. Chae, W. H. Lee, Y.-J. Ko, K. H. Chae, H.-s. Oh, U. Lee, D. K. Lee, B. K. Min, H. Shin, Y. J. Hwang and D. H. Won, Synergistic bimetallic CuPd oxide alloy electrocatalyst for ammonia production from the electrochemical nitrate reaction, *J. Mater. Chem. A*, 2022, **10**, 23760-23769.
5. X. Liu, X. Xu, F. Li, J. Xu, H. Ma, X. Sun, D. Wu, C. Zhang, X. Ren and Q. Wei, Heterostructured Bi_2S_3/MoS_2 nanoarrays for efficient electrocatalytic nitrate reduction to ammonia under ambient conditions, *ACS Appl. Mater. Interfaces*, 2022, **14**, 38835-38843.
6. J. Yang, H. Qi, A. Li, X. Liu, X. Yang, S. Zhang, Q. Zhao, Q. Jiang, Y. Su, L. Zhang, J.-F. Li, Z.-Q. Tian, W. Liu, A. Wang and T. Zhang, Potential-driven restructuring of Cu single atoms to nanoparticles for boosting the electrochemical reduction of nitrate to ammonia, *J. Am. Chem. Soc.*, 2022, **144**, 12062-12071.
7. M. Jiang, A. Tao, Y. Hu, L. Wang, K. Zhang, X. Song, W. Yan, Z. Tie and Z. Jin, Crystalline modulation engineering of Ru nanoclusters for boosting ammonia electrosynthesis from dinitrogen or nitrate, *ACS Appl. Mater. Interfaces*, 2022, **14**, 17470-17478.
8. F. Zhao, G. Hai, X. Li, Z. Jiang and H. Wang, Enhanced electrocatalytic nitrate reduction to ammonia on cobalt oxide nanosheets via multiscale defect

modulation, *Chem. Eng. J.*, 2023, **461**, 141960.

9. X. He, J. Li, R. Li, D. Zhao, L. Zhang, X. Ji, X. Fan, J. Chen, Y. Wang, Y. Luo, D. Zheng, L. Xie, S. Sun, Z. Cai, Q. Liu, K. Ma and X. Sun, Ambient ammonia synthesis via nitrate electroreduction in neutral media on Fe_3O_4 nanoparticles-decorated TiO_2 nanoribbon array, *Inorg. Chem.*, 2022, **62**, 25-29.
10. H. Guo, M. Li, Y. Yang, R. Luo, W. Liu, F. Zhang, C. Tang, G. Yang and Y. Zhou, Self-supported Pd nanorod arrays for high-efficient nitrate electroreduction to ammonia, *Small*, 2023, **19**, 2207743.
11. S. Zhang, M. Li, J. Li, Q. Song and X. Liu, High-ammonia selective metal-organic framework-derived Co-doped Fe/Fe_2O_3 catalysts for electrochemical nitrate reduction, *Proc. Natl. Acad. Sci. U.S.A*, 2022, **119**, e2115504119.
12. Y. Liu, B. Deng, K. Li, H. Wang, Y. Sun and F. Dong, Metal-organic framework derived carbon-supported bimetallic copper-nickel alloy electrocatalysts for highly selective nitrate reduction to ammonia, *J. Colloid Interface Sci.*, 2022, **614**, 405-414.
13. M. Jiang, J. Su, X. Song, P. Zhang, M. Zhu, L. Qin, Z. Tie, J.-L. Zuo and Z. Jin, Interfacial reduction nucleation of noble metal nanodots on redox-active metal-organic frameworks for high-efficiency electrocatalytic conversion of nitrate to ammonia, *Nano Lett.*, 2022, **22**, 2529-2537.
14. Z.-Y. Wu, M. Karamad, X. Yong, Q. Huang, D. A. Cullen, P. Zhu, C. Xia, Q. Xiao, M. Shakouri, F.-Y. Chen, J. Y. Kim, Y. Xia, K. Heck, Y. Hu, M. S. Wong, Q. Li, I. Gates, S. Siahrostami and H. Wang, Electrochemical ammonia synthesis via nitrate reduction on Fe single atom catalyst, *Nat. Commun.*, 2021, **12**, 2807.
15. H. Du, H. Guo, K. Wang, X. Du, B. A. Beshiwork, S. Sun, Y. Luo, Q. Liu, T. Li and X. Sun, Durable electrocatalytic reduction of nitrate to ammonia over defective pseudobrookite Fe_2TiO_5 nanofibers with abundant oxygen vacancies, *Angew. Chem. Int. Ed.*, 2022, **62**, e202215782.
16. Z. Niu, S. Fan, X. Li, P. Wang, Z. Liu, J. Wang, C. Bai and D. Zhang, Bifunctional copper-cobalt spinel electrocatalysts for efficient tandem-like nitrate reduction to ammonia, *Chem. Eng. J.*, 2022, **450**, 138343.

17. M. A. Akram, B. Zhu, J. Cai, S. Qin, X. Hou, P. Jin, F. Wang, Y. He, X. Li and L. Feng, Hierarchical nanospheres with polycrystalline Ir&Cu and amorphous Cu_2O toward energy-efficient nitrate electrolysis to ammonia, *Small*, 2023, **19, 2206966**.
18. W. Fu, Z. Hu, Y. Zheng, P. Su, Q. Zhang, Y. Jiao and M. Zhou, Tuning mobility of intermediate and electron transfer to enhance electrochemical reduction of nitrate to ammonia on Cu_2O/Cu interface, *Chem. Eng. J.*, 2022, **433**, 133680.
19. P. Hu, S. Hu, H. Du, Q. Liu, H. Guo, K. Ma and T. Li, Efficient electrocatalytic reduction of nitrate to ammonia over fibrous $SmCoO_3$ under ambient conditions, *Chem. Commun.*, 2023, **59**, 5697-5700.
20. X. Zhao, Q. Geng, F. Dong, K. Zhao, S. Chen, H. Yu and X. Quan, Boosting the selectivity and efficiency of nitrate reduction to ammonia with a single-atom Cu electrocatalyst, *Chem. Eng. J.*, 2023, **466**, 143314.
21. S. Lv, F. Gou, H. Wang, Y. Jiang, W. Shen, R. He and M. Li, Interface coupling of Ni_2P@Cu_3P catalyst to facilitate highly-efficient electrochemical reduction of nitrate to ammonia, *Appl. Surf. Sci.*, 2024, **648**, 159082.